Polymer Chemistry

ROYAL SOCIETY OF CHEMISTRY

PAPER

View Article Online
View Journal

Cite this: DOI: 10.1039/d0py01036g

Unraveling the gallol-driven assembly mechanism of thermoreversible supramolecular hydrogels inspired by ascidians†

Alexis Wolfel, [a,b] Esteban M. Euti,[a] Matías L. Picchio, *[a,c] Marcelo R. Romero, *[a] Victor M. Galván Josa,[b] Marisa Martinelli,[a] Roque J. Minari [d,e] and Cecilia I. Alvarez Igarzabal[a]

Received 20th July 2020,
Accepted 23rd October 2020

DOI: 10.1039/d0py01036g

rsc.li/polymers

Polyphenols-based supramolecular hydrogels have recently attracted much attention as smart materials for applications in several technologies. Although great advances have been made in this field, there is a challenging need for creating new versatile materials that combine synthesis simplicity and suitable functional properties. In this work, inspired by the hydrogen bonding ability of pyrogallol-bearing proteins found in ascidians, we explored a small gallol analog, gallic acid (GA), as a dynamic crosslinker of poly (vinyl alcohol) (PVA). The fundamentals of the supramolecular assembly mechanism of PVA/GA hydrogels are studied for understanding the final properties of the obtained thermo-reversible hydrogels. The polymer deacetylation degree was a key factor to control the gelation kinetics, morphology, and properties of the supramolecular materials. Furthermore, the intercalation of GA molecules between PVA chains produced polymer crystals with a new spatial arrangement, modifying the elastic modulus of the supramolecular network and increasing its stability in water. With remarkable fast gelation ability, ascidian-inspired PVA–GA hydrogels may provide a promising platform for a wide range of biomedical applications including topical drug delivery of therapeutic proteins, wearable electronic devices, and 3D printing.

1. Introduction

Supramolecular materials based on non-covalent interactions are of great interest for a wide range of biomedical applications owing to their unique properties such as stimuli-responsive gel/sol transition, toughness, easy processability, and shaping.[1–5] In the last decade, several studies have been aimed at developing multifunctional supramolecular materials inspired by living organisms.[6] For example, the outstanding underwater properties of marine mussel have driven a field of mussel-inspired catechol chemistry of great significance in biomaterials science and engineering.[7–17] Similar to mussels, ascidians are sac-like sessile marine animals that are covered with a protective membrane composed of highly crystalline cellulose nanofiber (tunicin) and proteins (tunichrome) containing 3,4,5-trihydroxyphenylalanine (TOPA) with a pyrogallol moiety (three hydroxyls bound to a benzene ring). These organisms have extraordinary biophysicochemical properties including rapid self-healing and strong adhesiveness in seawater.[18] Although the exact mechanism underlying these intrinsic features remains unclear, it is mainly associated with reversible H-bonding interactions between pyrogallol groups from TOPA together with metal–pyrogallol coordination, and pyrogallol-mediated oxidative covalent crosslinking.[19,20]

Recently, pyrogallol-containing polyphenols, such as tannic acid (TA),[21–23] epigallocatechin,[24,25] and epigallocatechin gallate,[26,27] among others, have gained great attention as building blocks for designing functional biomaterials. In particular, the multi-binding and metal ion coordination abilities of TA have been extensively exploited for the construction of supramolecular hydrogels with adhesive or shape memory behavior.[28–34] Conversely, small pyrogallol molecules have been less explored as hydrogelators and very few reports can be found in the literature.[35,36] Nandi *et al.* combined GA with a

[a]Departamento de Química Orgánica, Facultad de Ciencias Químicas (Universidad Nacional de Córdoba), IPQA–CONICET, Haya de la Torre y Medina Allende, Ciudad Universitaria, Córdoba X5000 HUA, Argentina. E-mail: mpicchio@santafe-conicet.gov.ar, marceloricardoromero@gmail.com
[b]Instituto de Física Enrique Gaviola, Facultad de Matemática, Astronomía y Física, CONICET, Medina Allende s/n, Córdoba 5000, Argentina
[c]Facultad Regional Villa María (Universidad Tecnológica Nacional), Av. Universidad 450, Villa María 5900, Argentina
[d]Instituto de Desarrollo Tecnológico para la Industria Química (INTEC), CONICET, Güemes 3450, Santa Fe 3000, Argentina
[e]Facultad de Ingeniería Química (Universidad Nacional del Litoral), Santiago del Estero 2829, Santa Fe 3000, Argentina

†Electronic supplementary information (ESI) available. See DOI: 10.1039/d0py01036g

low molecular weight compound, melamine, to obtain soft thermoreversible hydrogels *via* H-bonding interactions.[35] In addition, Lee *et al.* prepared self-healing hydrogels based on dynamic non-covalent interactions between pyrogallic acid and polyethylenimine.[36]

Alternatively, pyrogallol-conjugated polymers have recently emerged as biomimetic precursors for hydrogel formation in biomedical applications.[37,38] Indeed, pyrogallol-tethered chitosan,[19,20] hyaluronic acid (HA),[18,39,40] and gelatin (GEL)[41] hydrogels were prepared *via* oxidation-mediated covalent cross-linking, Fe^{3+} coordination, or multiple H-bonding interactions. Although these approaches showed to be highly efficient to obtain multifunctional supramolecular materials, the grafting of pyrogallol onto the polymers was demanded, requiring time and expensive chemicals.

In this context, we have recently reported a simple, rapid, and low-cost synthetic pathway for creating dynamic hydrogels by combining PVA with different small natural phenolic compounds.[42] These plant-derived molecules have reported antioxidant, antibacterial, anti-inflammatory, and anticancer properties,[43,44] resulting attractive for biomedical applications. However, a deeper understanding of the variables affecting the supramolecular assembly of these materials could lead to better control of the hydrogel properties, aiming to develop functional materials.

Herein, we report new supramolecular hydrogels, based on multiple non-covalent interactions between hydroxyl-rich PVA and GA, a small pyrogallol-containing compound that mimics the H-bonding ability of TOPA from ascidian proteins. Particular emphasis is given to understand the mechanism involved in the formation of these novel supramolecular structures. For that purpose, hydrogels were synthesized by using two kinds of PVA with different degrees of hydrolysis, in order to evaluate the influence of the presence of acetyl functional groups on the supramolecular gelation. We aimed to explore the chemistry of the supramolecular associations, the gelation kinetics, and the structural, viscoelastic, and mechanical features of the obtained materials to unveil their formation mechanism and their relationship with the degree of hydrolysis of the polymer precursor.

Moreover, owing to their strong dynamic interactions, the hydrogels were highly stretchable, thus mimicking the mechanical properties of soft tissues, and showed thermoreversible gelation. Therefore, these versatile hydrogels hold great potential as functional biomaterial platforms for 3D printing, tissue engineering, and topical drug delivery. Finally, this work not only enlightens the binding ability of GA but also opens new horizons to explore other naturally tailored small gallol analogs.

2. Materials and methods

2.1. Materials

Fully hydrolyzed PVA (Merck, degree of hydrolysis: ≥98.0%, M_w: 145 000), partially hydrolyzed PVA (ProtoKimica, degree of hydrolysis: 88.0%, M_w: 85 000), GA (Merck, ≥99.0%) and deuterium oxide (D_2O, Sigma-Aldrich, 99%) were used as supplied. PVA with a degree of hydrolysis ≥99.0% and M_w 85 000 was synthesized by alcoholysis of the partially hydrolyzed PVA following a method reported in the literature.[45] Deionized water was used for all experiments.

2.2. Preparation of PVA/GA supramolecular hydrogels

In a typical experiment, PVA (10 wt%) and GA (0.5–5 wt%) were dissolved under magnetic stirring in deionized water at 90 °C for 2 h. The prepared aqueous solutions (5 g) were poured into silicone molds (4 × 4 cm) and left at room temperature until spontaneous gelation. Pristine PVA hydrogels were prepared as a control by exposing polymer solutions to five cycles of freezing for 16 h at −20 °C and thawing for 8 h at 25 °C. The obtained materials were named PVA_x–GA_y, where x and y are the degree of hydrolysis of the polymer (%) and the GA concentration (wt%), respectively.

2.3. Microstructural studies

The internal morphology of swollen hydrogels was examined using a field emission scanning electron microscope (FE-SEM, ZEISS Sigma 300). For the test, the samples were swollen in water for 24 h, frozen in liquid nitrogen, and quickly lyophilized. Dry hydrogels were then coated with gold in a sputter coater and observed under an accelerating voltage of 2.0 kV.

2.4. Rheological analysis

Rheological studies were performed on an Anton Paar Physica MCR 301 rotational rheometer. The viscoelastic behavior of the supramolecular materials, in the dried or swollen state, was studied by using parallel-plate geometry (8 mm diameter). Prior to frequency sweep experiments, strain amplitude was varied from 0.01 to 20% at 1 Hz and 20 °C to determine the linear viscoelastic range (LVR) of the samples. Then, the frequency was varied from 0.1 to 100 Hz at 20 °C and a fixed strain of 0.1%.

Dynamic mechanical thermal analysis (DMTA) was also performed over xerogels and swollen gels. For dried samples, a parallel-plate 8 mm geometry was used and the temperature was varied from −25 to 200 °C with a heating rate of 2 °C min^{-1}, at 1 Hz of frequency, and 0.03% of strain amplitude. For swollen samples, a parallel-plate 25 mm geometry was employed and the temperature was varied in a heating/cooling cycle from 20 to 75 °C with a rate of 2 °C min^{-1}, at 1 Hz of frequency and 0.1% strain amplitude. In this last case, gel–sol and sol–gel phase transitions were determined as the temperature at which the storage modulus (G') equaled the loss modulus (G''), over heating and cooling runs, respectively.

Shear rate sweep tests were performed using a 50 mm diameter cone-plate geometry (0.05 mm gap) at 65 °C. Prior to the determinations, samples were fully dissolved by heating and stirring at 90 °C, and then were equilibrated for 5 min at 65 °C into the cone-plate geometry to eliminate thermal and shear histories. The sweep was carried over the range 0.1 to 1×10^4 rad s^{-1}.

2.5. Mechanical tests

Tensile and compression tests were carried out on an INSTRON 3344 testing machine. For the tensile tests, film specimens with a bone shape of length 9.53 mm and cross-section 3.18 mm × 1 mm were cut. Tests were carried out at 23 °C, 50% relative humidity, and an elongation rate of 25 mm min^{-1}. For compression tests, samples of around 1 mm thickness were subjected to a normal force, in which a 10 mm diameter plane-tip was moved down at a constant speed (1 mm min^{-1}), until compressing samples 65% their height.

2.6. Nuclear magnetic resonance spectroscopy (^{1}H-NMR)

Measurements were performed using a nuclear magnetic resonance spectrometer NMR Bruker Advance 400 MHz at 20 °C. Aiming to avoid bulk gelation, diluted PVA–GA solutions, with the same PVA/GA ratio of PVA_x-GA_5, were prepared in D_2O. Thus, PVA (1.7 wt%) and GA (0.85 wt%) were dissolved at 90 °C for 1 h, and then cooled down to room temperature. Solutions of pure components were identically prepared as a control. Since PVA_x–GA_5 samples showed the formation of a precipitate, all the solutions were centrifuged at 8500 rpm for 15 min prior to measurements. The following procedure was employed to semi-quantitatively calculate the mass of PVA and GA, which precipitated at room temperature, and the remaining mass in solution. Firstly, a careful weighing of the components (PVA and GA), during the sample preparation, was conducted to know the mass of the substances prior to precipitation. Next, after the heating (90 °C)/cooling (20 °C) process, where the dissolution (90 °C)/precipitation (20 °C) phenomenon took place, the samples were centrifuged and the supernatant was separated. Finally, a known amount of sodium benzoate was added as an internal standard into the supernatant solution and the mixture was measured by ^{1}H-NMR. To calculate the mass of the components in the mixture, the area under one of the sodium benzoate proton signals (7.91 to 7.84 ppm, $\int 1H$) was integrated and correlated with the known number of moles of the substance. Then, the amount of GA was determined by integrating the area under the aromatic proton signal (7.07 to 7.13 ppm, $\int 2H$). For PVA mass calculation, the area between 3.79 and 4.12 ppm was integrated, which is related to $\int 1H$ per repetitive unit of vinyl alcohol. Furthermore, the mass contributed by vinyl acetate repetitive units was added by considering the 12/88 or 2/98 factors, according to the polymer degree of hydrolysis.

2.7. Fourier transform infrared spectroscopy (FTIR)

FTIR spectra of the materials were recorded on a Nicolet iN10 (Thermo Fisher Scientific) infrared microscope in the range of 4000–400 cm^{-1}. Measurements were obtained from 30 scans with a resolution of 4 cm^{-1}.

2.8. X-ray powder diffraction (XRD)

Powder samples were analyzed on a Philips PW1800 diffractometer, with Cu Kα X-ray radiation, Si monochromator, at 40 kV and 30 mA, 0.3° min^{-1} scan, and 0.02° 2θ step size. Samples were mounted on a low background Si holder. Crystalline phases were identified and quantified by the Rietveld method implemented in the DiffracPlus TOPAS® software.

2.9. Swelling behavior of the supramolecular hydrogels

For swelling studies, dry discs of 10 mm diameter were immersed in beakers containing 5 mL of water at 25 °C. The discs were removed from the media at different time intervals, superficially dried with tissue paper, weighed, and then returned into the water container. Then, the degree of swelling (DS_t) was determined according to eqn (1), where W_s and W_d are the weight of the swollen and dry sample, respectively. This procedure was carried out in duplicate and until DS_t achieved the equilibrium (DS_e).

$$DS_t = (W_t - W_d)/W_d \times 100 \quad (1)$$

To determine the total soluble matter (TSM) of the materials during swelling, samples were carefully weighed in the dried state and re-swollen for 72 h in 5 mL of water. Later, the hydrogels were carefully dried at 37 °C until a constant weight was reached. Finally, the TSM was calculated as the percentage of lost mass between the xerogels before and after re-swelling.

2.10 Thermal analysis

Differential scanning calorimetry analysis was performed using heat/cool/heat cycles with a rate of 10 °C min^{-1} from −25 to 180 °C employing a DSC Q2000 equipped with the cooling system RSC90 (TA Instruments). Dried samples of 8–10 mg were weighed and placed into a hermetically sealed aluminum pan (TZero Technology). Nitrogen was used as a purging gas and the sample chamber was flushed at a flow rate of 50 mL min^{-1}. Glass transition temperature (T_g) was determined using the TA Universal Analysis software.

The thermal stability of the materials was studied by thermogravimetric analysis (TGA) on a TGA Q500 thermobalance (TA Instruments). Samples (3 mg) were heated from 40 to 600 °C with a heating rate of 10 °C min^{-1} under a nitrogen atmosphere (100 mL min^{-1}). The temperature at the main peak of the derivative weight loss curve was considered as the maximal decomposition rate ($T_{d_{max}}$).

2.11. Dynamic light scattering (DLS)

DLS experiments were performed at 25 °C using a Nano-ZS 90 Malvern equipment with a He–Ne laser (λ = 633 nm). PVA (1.7 wt%) and GA (0.4 wt%) were dissolved in water at 90 °C for 1 h. Then, the solutions were maintained at 25 °C for 20 h prior to DLS measurements in order to verify the sample stability. At the GA concentration used, the formation of the precipitate in the samples was not evidenced.

3. Results and discussion

3.1 PVA–GA supramolecular hydrogel formation

Supramolecular hydrogels were prepared by a one-pot approach, schematically shown in Fig. 1A, mimicking the pyrogallol chemistry of ascidians. Upon heating, PVA/GA mixtures were dissolved to yield a yellowish liquid which remained with no apparent further changes during the heating process. However, when PVA/GA solutions were cooled to room temperature, stretchable gels were spontaneously formed (Fig. 1B). Noteworthily, the formation of supramolecular networks between GA and PVA showed marked differences depending on the degree of hydrolysis of the polymer. Upon cooling to room temperature, PVA_{98}–GA_5 achieved the gel state in less than 10 minutes, while PVA_{88}–GA_5 needed about 5 h (see Video S1 of the ESI†). Furthermore, both supramolecular gels showed thermoreversibility (see Video S2 of the ESI†). Interestingly, in addition to the faster gelation kinetics, PVA_{98}–GA_5 hydrogel showed low gel–sol and sol–gel transition temperatures of 70 and 50 °C, respectively (Fig. 1C). In contrast, PVA_{88}–GA_5 showed a lower gel–sol transition temperature of around 50 °C, while the sol–gel transition could not be detected under the DMTA measurement conditions due to the slow gelation kinetics of this system (Fig. 1D). It is worth noting that both PVA_{98}–GA_5 and PVA_{88}–GA_5 hydrogels displayed hysteresis of the phase transition temperatures with $T_{gel-sol} > T_{sol-gel}$, which could be attributed to different sol–gel and gel–sol activation energies.[46]

Clearly, the PVA acetylation degree plays an important role in the assembly mechanism of the supramolecular network, which is reflected in the gelation kinetics and transition temperature. In order to understand this effect, the chemistry, microstructure, and physicochemical properties of both hydrogels were studied, aiming to reveal the global mechanism driving the polymer/pyrogallol supramolecular assembly.

3.2 Polymer/gallol supramolecular interactions

^{1}H-NMR studies were performed in order to identify the nature of the molecular interactions taking place after GA addition. The aromatic protons of GA appeared as a unique singlet signal at 7.1 ppm (Fig. 2A). In addition, PVA_{98} and PVA_{88} characteristic signals were identified: 3.79–4.12 ppm (–CH– in the backbone), 1.37–1.85 ($-CH_2-$ in the backbone), and 2.0–2.2 ppm ($-CH_3$ from acetate pendant groups) (Fig. 2B and D). According to the earlier mentioned results, a distinctive behavior was observed between PVA_{98}–GA_5 and PVA_{88}–GA_5. Although all samples were prepared under dilute conditions, PVA_{98}–GA_5 quickly showed turbidity upon cooling the sample to room temperature. On the other hand, PVA_{88}–GA_5 remained as a translucent liquid with a little precipitate, at least for 24 h. To avoid the inhomogeneities inserted by the phase-separated precipitates in the samples, all the mixtures were centrifuged

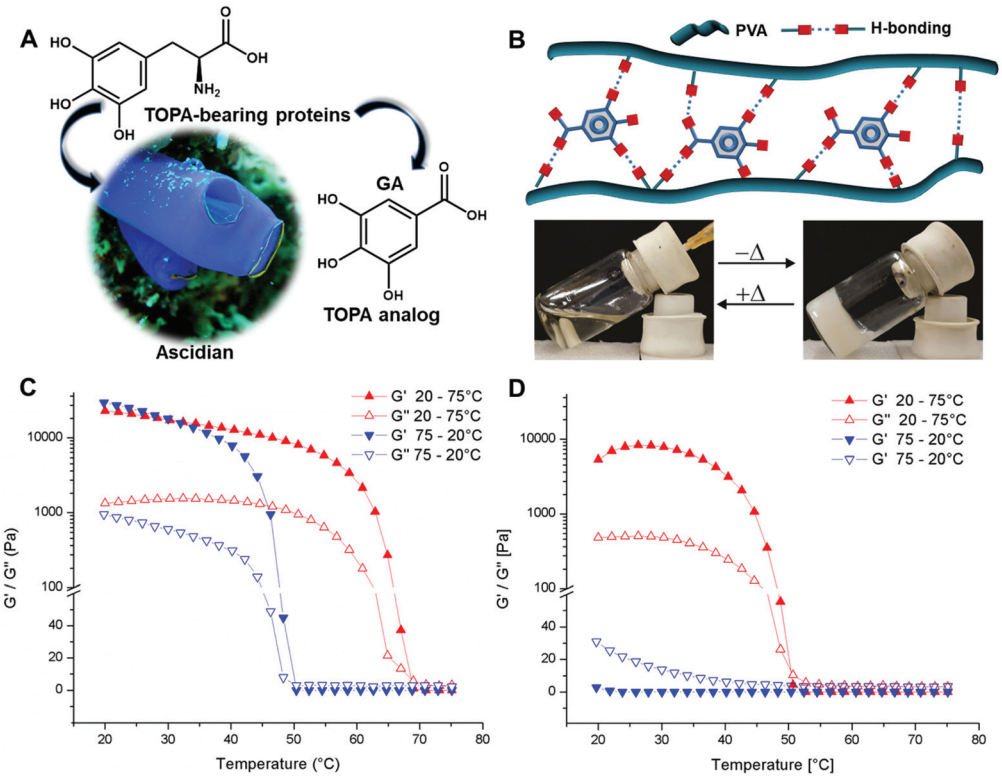

Fig. 1 (A) Chemical structure of the TOPA amino acid found in ascidian proteins and the pyrogallol analog GA. (B) Schematic representation of thermo-reversible hydrogel formation. (C) Evolution of the dynamic moduli of PVA_{98}–GA_5 and PVA_{88}–GA_5 (D) over heating/cooling cycles.

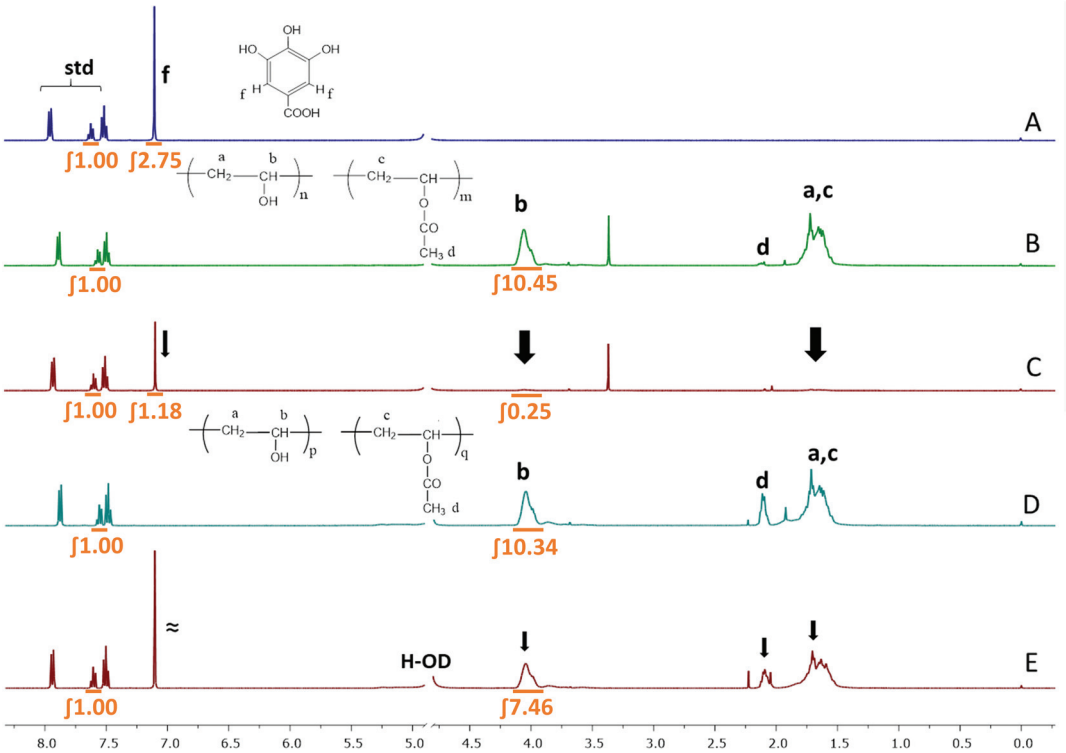

Fig. 2 ^{1}H-NMR spectra of (A) GA, (B) PVA_{98}, (C) PVA_{98}–GA, (D) PVA_{88} and (E) PVA_{88}–GA. Black arrows indicate a relative decrease in the signals. [PVA] = 1.7 wt%, [GA] = 0.4 wt%.

after the thermal equilibrium at room temperature was achieved. Thus, ^{1}H-NMR determinations were performed over supernatants (Fig. 2C and E) with an internal standard of sodium benzoate (std), which allowed us to obtain relevant information about still soluble species. As can be noted in Fig. 2C and E, the pattern of aromatic protons of GA was not modified after heating in the presence of PVA, indicating the absence of esterification reactions that could form covalent crosslinks. Therefore, we confirmed that the GA-assisted PVA gelation was driven by multiple non-covalent interactions.

Curiously, in PVA_{98}–GA_5 mixtures, the initial GA mass diminished around 60% (Fig. 2C) after the precipitation of the PVA_{98}/GA aggregates; additionally, the PVA signals almost disappeared, only retaining 2% of remnant polymer in solution. Therefore, the mass balance indicates that the precipitated supramolecular complex was composed of 77 wt% of PVA and 23 wt% of GA. In contrast, a slight amount of precipitate was found after PVA_{88}–GA_5 centrifugation, which correlates with a decrease in the initial phenolic acid and polymer masses of 24% and 36%, respectively. Consequently, the composition of the PVA_{88}–GA_5 solid complex was 78 wt% of the polymer and 22 wt% of the phenolic compound. It should be noted that despite the smaller amount of precipitate found in PVA_{88}–GA_5, in contrast to the PVA_{98}–GA_5 system, the final compositions of both supramolecular complexes were fairly similar, suggesting that acetate pendant groups effectively affect the kinetics but not the binding stoichiometry by mass. Considering the molar composition of the supramolecular complexes, we estimated that around 255 and 141 GA molecules were bound to one molecule of hydrolyzed and acetylated polymers, respectively. From these NMR data, the associative equilibrium constant (K_{eq}) of the supramolecular complexes was calculated through eqn (2), which relates the concentrations of associated and dissociated species. The obtained K_e values were 9×10^2 and 2×10^2 M^{-1} for PVA_{98}–GA_5 and PVA_{88}–GA_5, respectively.

$$K_e = \frac{[PVA - GA]}{[PVA][GA]} \quad (2)$$

Subsequently, the PVA/GA interactions were analyzed by FTIR. Pure GA and PVA_{98} spectra are shown in Fig. 3A and B. As can be observed, the phenolic acid exhibited three characteristic peaks at 1710 cm^{-1} (carboxylic acid), 1616 cm^{-1} (C=C stretching), and 1210 cm^{-1} (Ar–C–OH stretching) (Fig. 3A). For PVA_{98}–GA_5, the carbonyl signal at 1681 cm^{-1}, a shoulder at 1210 cm^{-1}, and a band widening at 3340 cm^{-1}, belonging to hydroxyl groups, were attributed to the presence of GA in the supramolecular materials (Fig. 3C). The signal at 1210 cm^{-1}, belonging to three Ar–C–OH functional groups, did not show a significant shifting with respect to the pure phenolic compound. However, the carbonyl signal found in PVA_{98}–GA_5 (1681 cm^{-1}) displayed a marked shifting of 29 cm^{-1} associated with strong hydrogen bonds probably originated from interactions with hydroxyl groups of PVA_{98}. In the case of PVA_{88}–GA_5 (Fig. 3E), the main signals associated with C=O are observed at 1714 and 1733 cm^{-1}, which correspond to the car-

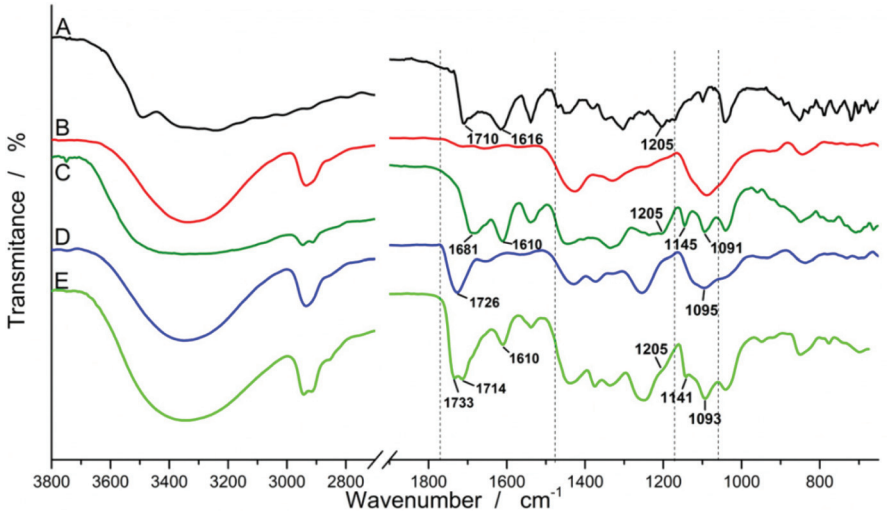

Fig. 3 FTIR spectra of (A) GA, (B) PVA_{98}, (C) PVA_{98}–GA_5, (D) PVA_{88} and (E) PVA_{88}–GA_5.

boxylic acid and acetate groups from GA and PVA_{88} (Fig. 3D), respectively. The absence of shifting in the carbonyl signals in PVA_{88}–GA_5 suggests that the association principle of GA with the acetylated polymer is manifested to a different extent compared to that in PVA_{98}–GA_5.

Remarkably, we found that PVA/GA samples showed signal ratios at 1140/1095 cm^{-1} (stretching C–OH vibrations) higher than pure polymers. This increase, which was particularly notable for PVA_{98}, has been frequently associated with an increase in the crystallinity of the polymer matrix.[47] Accordingly, FTIR analysis suggests that GA may induce the self-assembly of PVA chains in an ordered semi-crystalline structure.

In order to shed more light on this hypothesis, we analyzed the crystallographic structure of the supramolecular materials by XRD. As can be seen in Fig. 4A-1, GA showed a highly crystalline structure, according to its intense diffraction signals. Notably, the addition of GA increases the global crystallinity of the system PVA/GA (Fig. 4A-2 and A-3), though the diffraction signals found do not correspond to pure GA crystals inside the polymer. More intriguingly, these signals neither coincide with the diffraction pattern of pure PVA crystals (Fig. 4A-4 and A-5), which seem to be present at a low proportion in the supramolecular samples. Clearly, these results can only be explained by a new molecular organization that controls the crystalline conformation in the supramolecular structures. These new crystal arrangements could be formed by structures that incorporate GA molecules strongly interacting with PVA chains, giving more ordered molecular domains. Note that acetate groups in PVA_{88} could affect the interaction and the alignment of chains giving less intense signals, but not affect the nature of the crystals, which show very similar θ (see Fig. 4A-2). These crystalline structures (PVA_{98}–GA_5 and PVA_{88}–GA_5) are not reported in the literature, and a complete Crystallographic Information File (CIF) is not available. Therefore, both structures were analyzed by implementing the LeBail analysis[48] (whole powder pattern

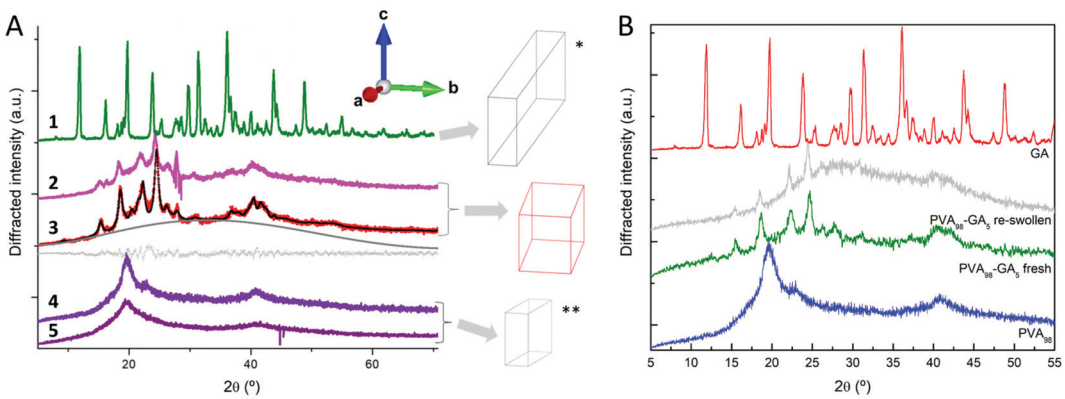

Fig. 4 XRD patterns of the materials. (A) (1) GA, (2) PVA_{88}–GA_5, (3) PVA_{98}–GA_5, (4) PVA_{98}, and (5) PVA_{88}. Arrows indicate the schematic representation of unit cells of the different materials. In curve 3: LeBail fitting (black), fitted background (dark gray), and residual (light gray). *Reported by Fronczek *et al.*[50] **Reported by Bunn.[51] (B) Comparison of freshly prepared PVA_{98}–GA_5 with dried/re-swollen hydrogels.

decomposition method). An initial estimation for the space group and lattice parameters was obtained with the Treor routine available in the Fullprof Suite software.[49] The peak shape was modeled by the fundamental parameters approach (FPA) implemented in TOPAS®, which involves the convolution of physical models of each component (slits, monochromator, source emission profile, *etc.*) to generate the XRD peak profiles.

As reported in the literature, pure GA and PVA crystallize in the monoclinic systems $C2/c$ [50] and $P21/m$,[51] correspondingly. According to the XRD analysis performed, the samples PVA_{88}–GA_5 and PVA_{98}–GA_5 crystallize in the space group $P12_1/c1$ with the following lattice parameters: a = 8.641 (3) Å, b = 9.651 (2) Å, and c = 10.199 (2) Å and β = 122.09° (1). In addition, the crystal size domains were determined with the LeBail method, being 12 (1) nm for PVA_{98}–GA_5 and 5 (1) nm for PVA_{88}–GA_5. The goodness-of-fit (GOF), which resulted in 1.32, was defined as:

$$\mathrm{GOF} = \sqrt{\frac{1}{N-P}\sum_{i=1}^{N}\frac{(Y_i-\tilde{Y}_i)^2}{Y_i}}$$

where Y_i are experimental intensities and $\tilde{Y}_i$ are predicted intensities for the i-th channels; i denotes each one of the N channels in the considered XRD pattern, and P is the number of free parameters in the fitting process. A GOF equal to 1 represents a perfect fit.

In contrast with Wang *et al.*,[31] which reported that multifunctional polyphenol TA strongly interacts with PVA preventing the formation of polymer crystallites, our XRD results indicate that both PVA–GA supramolecular structures were ordered in a similar fashion at the angstrom level, but a lower quantity of crystals is present when the number of acetyl groups increases in the polymer backbone. This fact suggests that acetyl groups could hamper the macromolecular organization to some extent.

One key question arising from these results is related to the formation of semi-crystalline domains: are they the result of hydrogel drying or formed during hydrogel preparation? In order to address this point, XRD patterns of freshly prepared and re-swollen hydrogels were studied. PVA_{98}–GA_5 was chosen for this analysis as it shows the highest crystallinity in dry state.

Strikingly, the crystalline structures were also found in freshly prepared PVA_{98}–GA_5 hydrogels (Fig. 4B). Moreover, after drying the samples and re-swelling in an excess of water for 72 h, the crystalline domains still remained. These findings suggest that the crystallites are formed during the hydrogel preparation (probably during the cooling process) and could play an important role in gelation and in the swelling and mechanical stability of the yielded materials.

3.3 Structural and viscoelastic properties of PVA–GA supramolecular materials

Aiming to determine the macroscopic properties of supramolecular polymers and gain insight into the PVA/GA organization, FE-SEM, rheology, and swelling tests were carried out.

As is well known, the acetylation degree of PVA is determinant for the formation of pure PVA hydrogels through freezing–thawing processing.[52] Accordingly, the obtained PVA_{98} hydrogels showed a porous structure, as observed by SEM (Fig. 5A and B). In contrast, PVA_{88} was unable to yield hydrogels and showed a fairly homogeneous internal morphology (Fig. 5C and D). More importantly, the addition of GA to yield supramolecular structures promoted large differences compared with the pure polymers. Both PVA_{88}–GA_5 and PVA_{98}–GA_5 supramolecular hydrogels exhibited a highly porous morphology regardless of the zone explored in the material (Fig. 5E, F, and G, H). However, PVA_{98}–GA_5 showed poorly-interconnected bigger globular structures of around 500 nm (Fig. 5G and H). This difference is undoubtedly correlated with the differential gelation kinetics previously observed and therefore with the supramolecular assembly mechanism between PVA and GA.

The obtained PVA/GA supramolecular hydrogels showed good mechanical properties with high stretchability and resistance to compression (see Fig. S1 in the ESI†). Moreover, these properties differed according to the polymer acetylation degree. Young's modulus, tensile strength, and elongation at break were around 200 and 20 kPa, 217 and 17 kPa, and 500 and 130% for PVA_{88}–GA_5 and PVA_{98}–GA_5, respectively (Fig. S1A†). On the other hand, both PVA_{88}–GA_5 and PVA_{98}–GA_5 hydrogels resisted the compression test without failure with similar compression stress, close to 154 kPa at 65% of compression strain (Fig. S1B†). These results can be correlated to the chemical nature of the networks and its structural arrangement at the mesoscale, resulting from the extremely different gelation kinetics of both systems, as was previously shown in Video S1 of the ESI.† In this sense, it is noteworthy that PVA_{98}–GA_5 was formed quickly in relation to PVA_{88}–GA_5. This fast gelation probably led to soft macroscopic structures as a consequence of a low-interconnected morphological organization (see Fig. 5G and H). Conversely, the addition of GA to PVA_{88} promotes a slow gelation process with a better-interconnected structure of superior mechanical properties. In addition, the presence of hydrophobic arrangements within PVA_{88}–GA_5, due to a larger amount of acetyl functional groups, could contribute to the larger stretchability of this hydrogel.[53] Then, the viscoelastic properties of these new materials were analyzed in dry and hydrated states. The frequency sweep test performed over dried samples (Fig. 6A) did not show significant differences in the elastic moduli (G', an average value of 3×10^3 Pa) for pure PVA with different degrees of hydrolysis, indicating similar molecular packing in the polymer networks. However, PVA–GA supramolecular materials showed very dissimilar behaviors depending on the polymer degree of hydrolysis. In PVA_{98}–GA_5, the presence of the phenolic acid produced a G' reduction down to 5×10^2 Pa. In contrast, in the case of PVA_{88}–GA_5, a five times increase in G' in comparison with the pure polymer was observed. These results are in line with the previously discussed mechanical behavior and are mainly attributed to the microscopic organization of the materials at the mesoscale.

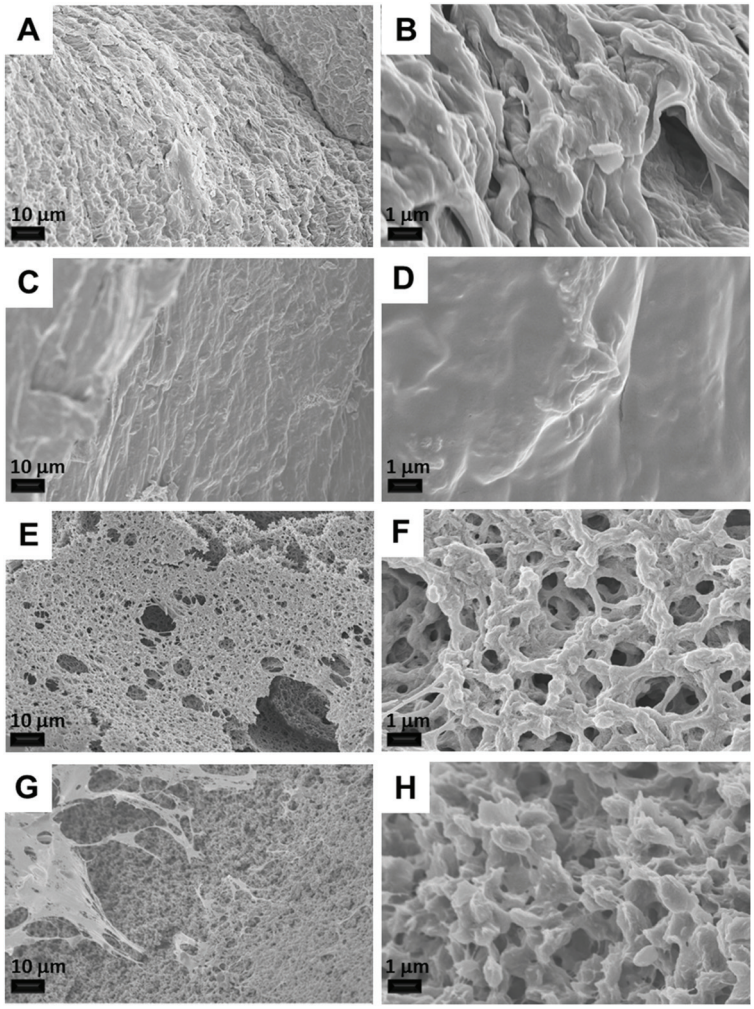

Fig. 5 SEM micrographs of PVA_{98} (A and B), PVA_{88} (C and D), PVA_{88}–GA_5 (E and F), and PVA_{98}–GA_5 (G and H) hydrogels at different magnifications (from left to right: 1000× and 10 000×).

The swelling behavior of the materials was also studied, since it may be related to the structure and hydrophilicity of the network. PVA and PVA–GA samples were dipped in water and the mass changes were followed to determine the DS_t over time (Fig. 6B). As can be seen, the PVA_{88} xerogel was quickly solubilized during the determination, in comparison with PVA_{98} that resisted the swelling experiment. The more hydrolyzed polymer is known to reach a highly ordered crystalline structure which remains relatively stable under the polymer swelling. Thus, after swelling in water, the mass increased by 250%. In contrast, acetyl functional groups of PVA_{88} restrict the formation of enough crystalline domains, thus yielding a soluble network. Interestingly, when GA was added to PVA_{88}, the supramolecular material withstands its solubilization giving a response similar to pristine PVA_{98} during the first 7 h of the test, and then it became a really soft material. Indeed, after swelling for 72 h, the TSM of this material was 32%. Furthermore, PVA_{98}–GA_5 showed a very low swelling degree, six times lower than PVA_{98}, and a TSM value of 15%. These results indicate that the incorporation of GA gave rise to new attractive interactions resulting in less swellable materials. These strong interactions, which act as crosslinking points preventing material solubilization, could be correlated with the ordering of the polymer and phenolic molecules in new crystalline arrangements, as was observed by XRD.

Moreover, re-swollen samples of PVA_{98}, PVA_{88}–GA_5, and PVA_{98}–GA_5 showed a marked reduction in their elastic moduli (Fig. 6C) with respect to dried samples. Thus, PVA_{88}–GA_5 which behaved as a strong and elastic polymer in the dry state became a soft material after swelling in water, probably due to the easier intercalation of the solvent between the acetylated polymer chains of low crystallinity. On the other hand, PVA_{98}–GA_5 experienced less mechanical changes after swelling, and its elasticity was practically unaltered from dry to swollen state.

Additionally, in the analyzed frequency range (0.1 to 100 Hz), the elasticity was kept practically constant, indicating strong interactions that resemble a network of infinite size with long relaxation time (>10 s). Despite their near-covalent viscoelastic behavior, pyrogallol-based hydrogels have revers-

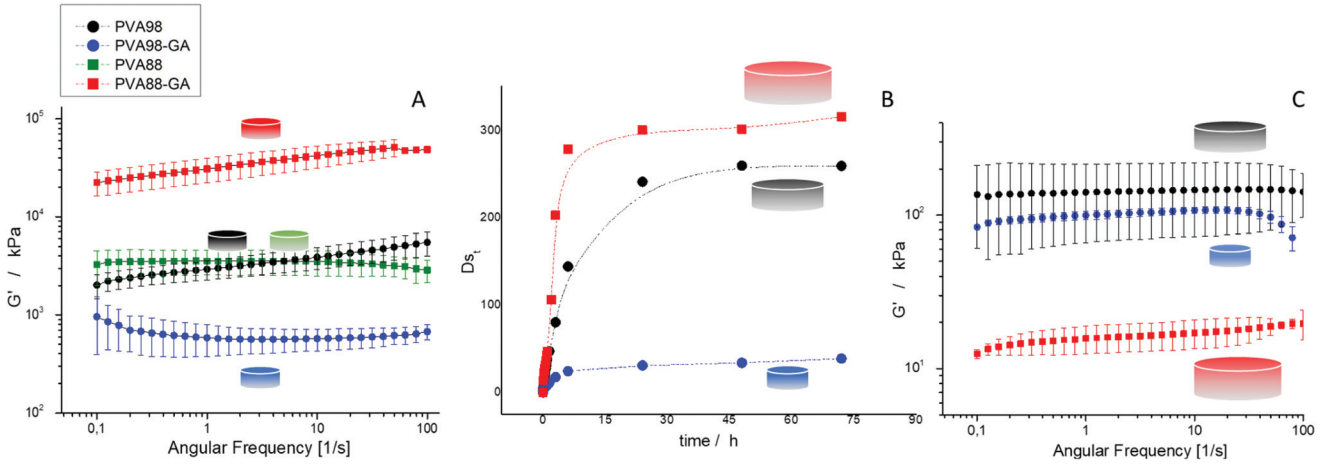

Fig. 6 (A) *G′ vs.* frequency for xerogels. (B) Swelling tests of the hydrogels in water. (C) Viscoelastic behavior of the swollen materials.

ible phase transition temperatures suitable for printing applications. Overall, the above results show that PVA–GA supramolecular hydrogels present good mechanical strength even under a water-swollen state, suggesting that these materials have potential as scaffolds for biomedical applications.

3.4 Thermal behavior of PVA–GA supramolecular networks

Aiming to study the effect of the PVA–GA structure on the thermal behavior of the developed materials, thermogravimetric analyses were carried out. As shown in Fig. 7, when the samples were heated up to about 100 °C, the mass decrease was attributed to the loss of solvation water. In addition, a detailed analysis indicated that in PVA_{98} and PVA_{98}–GA_5, this process began at around 80 °C, while for PVA_{88} and PVA_{88}–GA_5, the loss of water occurred from 50 °C. Water retention in the polymer network is therefore more dependent on the PVA degree of hydrolysis than on the GA intercalation. In addition, PVA_{98} presented one main decomposition peak at 280 °C (76%), while PVA_{88} degradation occurred in two steps, the first one at 326 °C (57%) and the other one at 424 °C (28%), as previously reported in the literature.[54] Interestingly, the samples containing GA present a new decomposition process at a lower temperature than pure PVA. In these thermal processes, the mass percentage decreased by 36 and 23% at temperatures of 219 and 222 °C for PVA_{88}–GA_5 and PVA_{98}–GA_5, respectively. These mass losses are associated with the GA decomposition, although they occur at 20 °C lower than the pure phenolic acid, according to TGA studies reported elsewhere.[55] In order to obtain more insight into this phenomenon, DSC studies were simultaneously compared. As can be observed in Fig. 7, PVA_{88} and PVA_{98} presented endothermic melting processes (T_m) at 219 and 222 °C, respectively, while the new crystalline domains in the PVA–GA supramolecular networks melted at 113 and 132 °C, for the acetylated and hydrolyzed polymers. Curiously, T_m of the pure polymers exactly agrees with the decomposition temperature of the phenolic acid in PVA–GA materials. We hypothesized that the lower decomposition temperature of GA than that observed for the pure phenolic acid could be a consequence of a combination of two factors. First, GA is present in the supramolecular PVA–GA matrix in a lower degree of self-association than in its pure state, which makes this phenolic acid less resistant to thermal decomposition. Second, T_m of the pure polymers exactly agrees with the decomposition temperature of the phenolic acid in PVA–GA materials. Therefore, the molecular motion reached by the polymer chains at T_m of the remaining PVA crystallites in the PVA–GA structure allowed a transfer of thermal energy towards the GA molecules, which could induce their decomposition at a lower temperature than the pure phenolic acid. Unfortunately, the presence of PVA semi-crystalline domains could not be assessed by DSC since the supramolecular networks showed early decomposition with a significant mass loss before the T_m of pure PVA.

The subsequent decomposition processes at higher temperatures accentuate even more the differences between PVA–GA supramolecular materials with different degrees of hydrolysis. Two processes occur in PVA_{88}–GA_5, one of larger magnitude and over a wide temperature range, centered at 334 °C (36%) and another smaller one at 435 °C (13%). In contrast, PVA_{98}–GA_5 presents significant decomposition in a narrow temperature range, centered at 312 °C (43%), along with a negligible degradation at 430 °C (4%). Thus, the decomposition temperatures of PVA_{88}–GA_5 are similar to those observed in PVA_{88}. For this reason, we believe that the stabilizing effect provided by the acetate groups in pure PVA was also extended to the supramolecular materials. A brief summary of PVA–GA thermal properties has been schematized at the top of Fig. 7. In the proposed structure, PVA–GA supramolecular materials contain combined phenol–polymer arrangements. After heating the material above T_m of PVA–GA crystals, GA is freely delivered into the polymer network but remains in the ordered structure of pure PVA crystals. However, further heating over T_m of PVA crystals favors the molecular motion of polymer coils, which transfer their thermal energy promoting the total GA decomposition. Additional thermomechanical studies can be found in Fig. S2 of the ESI.†

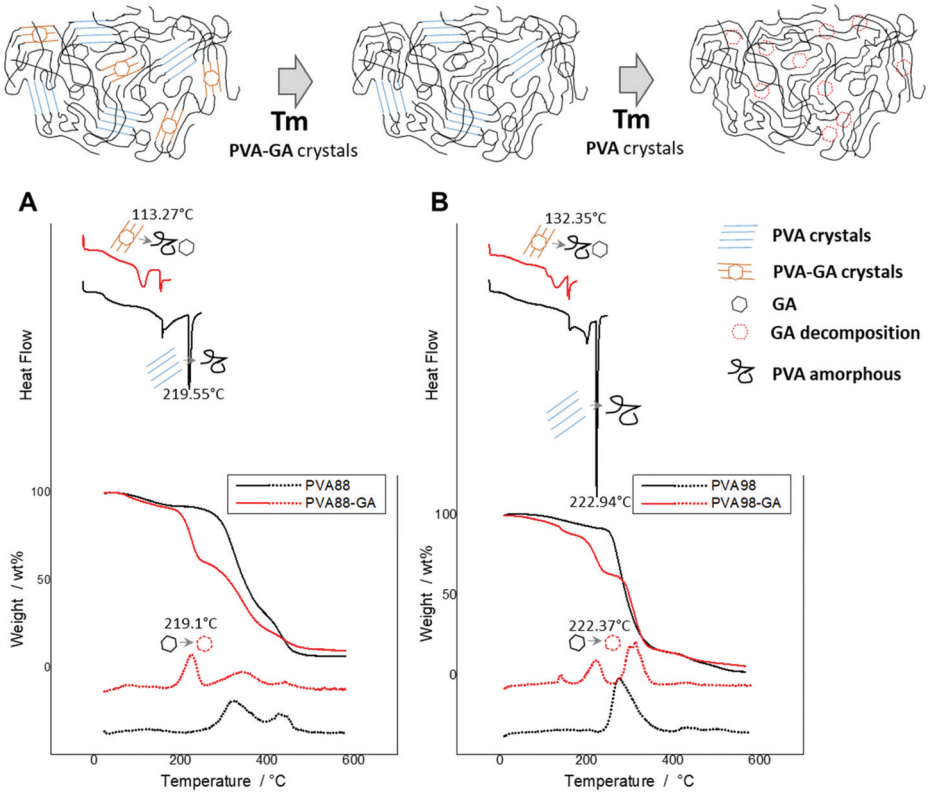

Fig. 7 TGA–DSC thermograms of (A) PVA_{88}, PVA_{88}–GA_5 and (B) PVA_{98}, PVA_{98}–GA_5.

3.5 Assembly mechanism for the PVA/gallol supramolecular structures

Together with the previously gathered information, DLS measurements and molecular dynamic simulations were performed to unravel the supramolecular arrangement pathway between PVA and GA (Fig. 8). For an adequate DLS analysis, samples were diluted approximately 6 times. DLS studies showed that the initial PVA solutions contain PVA_{88} and PVA_{98} coils of 20 nm and 30 nm, respectively (for further details, see Fig. S3 of the ESI†). Then, in the presence of GA, the differences in the properties of both materials were surprisingly amplified by the formation of supramolecular assemblies. One of the first differences was manifested in the gelation kinetics of PVA_{88}–GA_5 and PVA_{98}–GA_5. As shown in the experiments of Video S1,† a fast color change occurred in both samples during the cooling process, indicating the nucleation of PVA with GA. In this step, PVA_{88}–GA_5 showed particles with 35 nm diameter, as determined by DLS (Fig. 8A). However, the respective PVA_{98}–GA_5 particles were not possible to measure with an acceptable accuracy due to the instantaneous gelation promoted by GA, which yielded a whitish product (Fig. 8B), even when it was attempted to measure under dilute conditions (see Fig. S3 of the ESI†). Moreover, gelation was not reached at the same time in PVA_{88}–GA_5 (Fig. 8A) and it took about 5 h to yield a gel. Clearly, these different kinetic processes conditioned the microscopic organization of the materials, conferring them different properties as was previously demonstrated. However, a question remained regarding the possible influence of the polymers' molecular weight used in this work (145 and 85 kDa for PVA_{98} and PVA_{88}, respectively) on the gelation times. For this reason, a small amount of PVA_{88} was hydrolyzed and the product (PVA_{99}, degree of hydrolysis >99%, as determined by FTIR spectroscopy, see Fig. S4 of the ESI†) had the same chain length as its predecessor, but with a different acetylation degree (equivalent to PVA_{98}). Then, kinetic experiments of supramolecular gelation were repeated with PVA_{99} and no significant differences were observed, compared with the previous results obtained by using PVA_{98} (see Video S3 of the ESI†). Only a small decrease in the gelation time (from 10 to 4 min) was observed for the highly-hydrolyzed low-molecular-weight polymer. Evidently, under the studied conditions, molecular weight is not dominant in the kinetic control of the supramolecular gelation.

The observed kinetics and structural differences in the supramolecular hydrogels could be explained by a model that takes into account the organization of the PVA polymer coils in aqueous solution and the affinity between the functional groups of GA with the macromolecules. In this regard, highly stable hydrogen-bonded complexes of GA-acetate groups were predicted by MMFF94 molecular dynamics simulations based on the force field calculation method[56] (see Fig. S5 of the ESI†).

Furthermore, a relevant characteristic of acetate groups in solvated PVA_{88} is their predominant distribution preferably oriented inside the polymer coils, and therefore less exposed

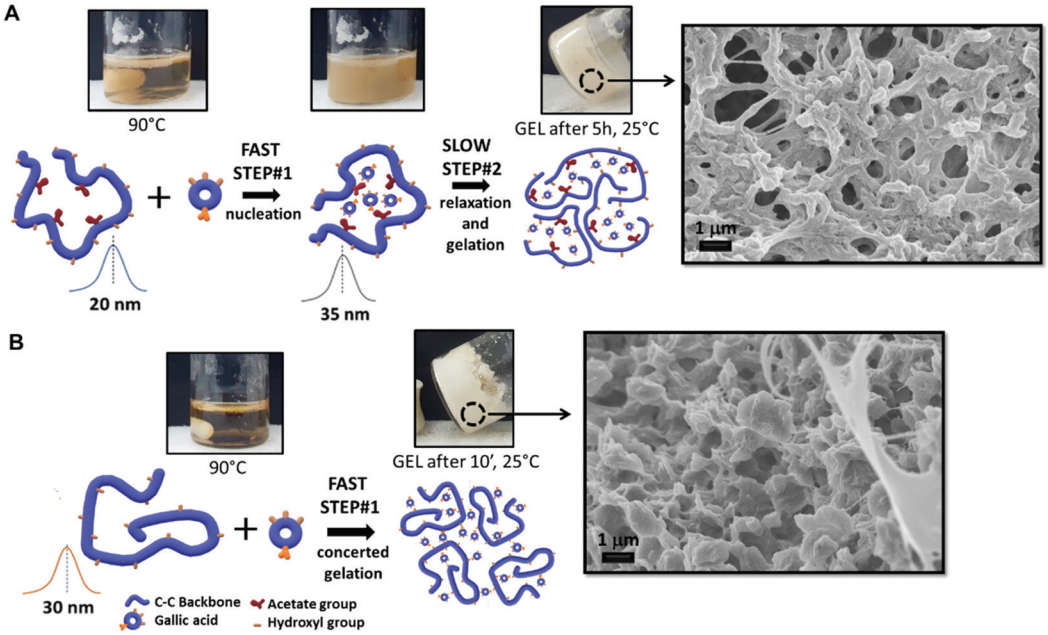

Fig. 8 Proposed mechanisms for PVA–GA gelation: (A) PVA_{88}–GA_5 gel is assembled in two steps, a fast formation of the polymer chain–GA supramolecular complex followed by a slow PVA–GA association to obtain a smooth non-porous network, after 5 h at 25 °C. (B) PVA_{98}–GA_5 gel is obtained after a concerted fast reaction giving globular shape structures, after 5 min at 25 °C.

to the solvent. In fact, this particular distribution of acetate moieties has been previously exploited to load hydrophobic molecules inside colloidal particles of PVA (poly(vinyl acetate)).[57] Such an acetate group distribution can determine the GA partition, based on the polymer nature, which would preferably be within the polymer coils in PVA_{88}, while it would be less localized in PVA_{98}. Taking into account the overall number of GA molecules (GA_t), added to prepare the supramolecular networks (eqn (3)), two kinds of assembly pathways could be considered.

$$GA_t = GA_i + GA_e \quad (3)$$

where GA_i is the GA fraction in the core of the polymer coils and GA_e represents the phenolic compound distributed and bonded on the external part of the polymer tangles. As a consequence, the availability of GA_e may be limited in the PVA_{88}–GA_5 complexes, handicapping the gelation process. Thus, we propose that in this system, the supramolecular assembly could occur during the cooling process in two steps: (i) PVA_{88}–GA_5 nucleation, followed by (ii) polymer relaxation and gelation (Fig. 8A). In contrast, for the PVA_{98}–GA_5 system, wherein polymer coils are decorated with a high concentration of GA_e, strong chain interactions are promoted and a crosslinked polymer network is formed in a concerted way (Fig. 8B). Additionally, the gelation kinetics of both assembly pathways is dependent on the GA_e concentration, and it could be represented by eqn (4):

$$\frac{1}{\tau_{sg}} \propto [GA_e] \quad (4)$$

where τ_{sg} is the supramolecular gelation time.

Indeed, we found a non-linear dependency of the gelation time on the GA concentration (see Video S4 of the ESI†). Thus, hydrogel formation took 10, 14, 55 min or around 24 h, when the amount of the pyrogallol monomer in PVA_{98}–GA materials varied from 5, 3, 1 to 0.5 wt%, respectively.

Therefore, τ_{sg} could control the supramolecular gel morphology. On the one hand, when the gelation proceeds at high speed, early phase separation occurs rapidly before chain unwinding, forming a highly globular porous structure. On the other hand, when the macromolecules have time to interact simultaneously with GA and each other, their microscopic morphology tends to reach more interconnected and homogeneous structures.

From these proposed gelation pathways, interesting deductions could be made about the crystalline structure of the supramolecular materials. It should be noted that regardless of the polymer degree of hydrolysis, the crystalline arrangements in the supramolecular structure with GA showed similar cell units, according to XRD studies. Therefore, since gelation proceeds at a different rate for each polymer, these crystals should be formed early when the supramolecular assembly started. Thus, the higher crystallinity observed in PVA_{98}–GA_5 compared with PVA_{88}–GA_5 indicates a greater degree of association in the former (which is supported by its superior K_e value, 9×10^2 *vs.* 2×10^2 M^{-1}), despite the fact that shorter times were necessary to give a macroscopic solid structure.

Finally, it is worth mentioning that the superior gelation rate obtained with PVA_{98}–GA_5 (10 min) could be particularly desirable for some engineered applications such as 3D

printing, wherein fast hydrogel formation is required after extrusion, or for topical drug delivery where the sol–gel transition should occur rapidly upon contact with the skin. For this reason, as a proof of concept, we studied the effect of the shear rate on the viscosity of PVA_{98}–GA_5 solution and its printability. As can be seen in Fig. S6,† the gelling solution showed shear thinning behavior at 65 °C and could be easily injected to print a predesigned filament arrangement (see Video S5 of the ESI,† where the word "GEL" was written). In sum, these results unveil the great potential of this supramolecular hydrogel to be employed in printing applications.

4. Conclusions

Thermoreversible PVA/GA supramolecular hydrogels were easily prepared through a one-pot hot-dissolution/cooling step. The assembly of the PVA chains in the presence of GA was explained by taking into account the organization of the PVA polymer coils in water and the affinity between the functional groups of phenolic compounds with the macromolecules. Strong interactions between PVA and GA changed the conformation of the pure polymer and promoted the precipitation of the molecular entanglements with defined composition, which agglomerate and compact into globular structures, favored by the interfacial tension. The presence of acetate groups hampers these arrangements, modifying the gelation kinetics and the final properties of the supramolecular hydrogels. In addition, the incorporation of GA gives rise to ordered polymer–phenol arrangements into the supramolecular networks, resulting in a higher density of crystals in the bulk, with a completely new spatial arrangement. These new crystalline domains were likely responsible for increasing the stability in water. Supramolecular materials here developed could be attractive in the field of biomaterials since GA can endow them with many favorable features such as antioxidant, anti-inflammatory, antimicrobial or antitumor properties. Although additional studies are ongoing, we anticipate that PVA–GA soft materials will open up a new avenue for the development of 3D-printable inks, wearable electronic devices, and redox-active polymer binders in the future.

Conflicts of interest

There are no conflicts to declare.

Acknowledgements

The authors acknowledge the financial support granted by CONICET, ANPCyT, SECyT (Universidad Nacional de Córdoba), Universidad Nacional del Litoral, and Universidad Tecnológica Nacional, all from Argentina.

References

1 E. A. Appel, J. Del Barrio, X. J. Loh and O. A. Scherman, Supramolecular polymeric hydrogels, *Chem. Soc. Rev.*, 2012, **41**, 6195–6214.
2 J. L. Mann, A. C. Yu, G. Agmon and E. A. Appel, Supramolecular polymeric biomaterials, *Biomater. Sci.*, 2018, **6**, 10–37.
3 G. Liu, Q. Yuan, G. Hollett, W. Zhao, Y. Kang and J. Wu, Cyclodextrin-based host–guest supramolecular hydrogel and its application in biomedical fields, *Polym. Chem.*, 2018, **9**, 3436–3449.
4 M. M. Perera and N. Ayres, Dynamic covalent bonds in self-healing, shape memory, and controllable stiffness hydrogels, *Polym. Chem.*, 2020, **11**, 1410–1423.
5 C. D. Spicer, Hydrogel scaffolds for tissue engineering: the importance of polymer choice, *Polym. Chem.*, 2020, **11**, 184–219.
6 C. Sanchez, H. Arribart and M. M. G. Guille, Biomimetism and bioinspiration as tools for the design of innovative materials and systems, *Nat. Mater.*, 2005, **4**, 277–288.
7 J. H. Ryu, P. B. Messersmith and H. Lee, Polydopamine Surface Chemistry: A Decade of Discovery, *ACS Appl. Mater. Interfaces*, 2018, **10**, 7523–7540.
8 H. Lee, S. M. Dellatore, W. M. Miller and P. B. Messersmith, Mussel-Inspired Surface Chemistry for Multifunctional Coatings, *Science*, 2007, **318**, 426–430.
9 B. M. Park, J. Luo and F. Sun, Enzymatic assembly of adhesive molecular networks with sequence-dependent mechanical properties inspired by mussel foot proteins, *Polym. Chem.*, 2019, **10**, 823–826.
10 L. Li, W. Smitthipong and H. Zeng, Mussel-inspired hydrogels for biomedical and environmental applications, *Polym. Chem.*, 2015, **6**, 353–358.
11 S. K. Madhurakkat Perikamana, J. Lee, Y. B. Lee, Y. M. Shin, E. J. Lee, A. G. Mikos and H. Shin, Materials from Mussel-Inspired Chemistry for Cell and Tissue Engineering Applications, *Biomacromolecules*, 2015, **16**, 2541–2555.
12 Q. Wan, M. Liu, J. Tian, F. Deng, G. Zeng, Z. Li, K. Wang, Q. Zhang, X. Zhang and Y. Wei, Surface modification of carbon nanotubes by combination of mussel inspired chemistry and SET-LRP, *Polym. Chem.*, 2015, **6**, 1786–1792.
13 M. Enke, R. K. Bose, S. Zechel, J. Vitz, R. Deubler, S. J. Garcia, S. Van Der Zwaag, F. H. Schacher, M. D. Hager and U. S. Schubert, A translation of the structure of mussel byssal threads into synthetic materials by the utilization of histidine-rich block copolymers, *Polym. Chem.*, 2018, **9**, 3543–3551.
14 M. Vatankhah-Varnoosfaderani, S. Hashmi, A. Ghavaminejad and F. J. Stadler, Rapid self-healing and triple stimuli responsiveness of a supramolecular polymer gel based on boron–catechol interactions in a novel water-soluble mussel-inspired copolymer, *Polym. Chem.*, 2014, **5**, 512–523.

15 J. Deng, C. Cheng, Y. Teng, C. Nie and C. Zhao, Mussel-inspired post-heparinization of a stretchable hollow hydrogel tube and its potential application as an artificial blood vessel, *Polym. Chem.*, 2017, **8**, 2266–2275.
16 S. Zhou, H. Ji, L. Liu, S. Feng, Y. Fu, Y. Yang and C. Lü, Mussel-inspired coordination functional polymer brushes-decorated rGO-stabilized silver nanoparticles composite for antibacterial application, *Polym. Chem.*, 2020, **11**, 2822–2283.
17 Z. Li, W. Lu, T. Ngai, X. Le, J. Zheng, N. Zhao, Y. Huang, X. Wen, J. Zhang and T. Chen, Mussel-inspired multifunctional supramolecular hydrogels with self-healing, shape memory and adhesive properties, *Polym. Chem.*, 2016, **7**, 5343–5346.
18 J. H. Cho, J. S. Lee, J. Shin, E. J. Jeon, S. An, Y. S. Choi and S. W. Cho, Ascidian–Inspired Fast–Forming Hydrogel System for Versatile Biomedical Applications: Pyrogallol Chemistry for Dual Modes of Crosslinking Mechanism, *Adv. Funct. Mater.*, 2018, **28**, 1705244.
19 N. D. Sanandiya, S. Lee, S. Rho, H. Lee, I. S. Kim and D. S. Hwang, Tunichrome-inspired pyrogallol functionalized chitosan for tissue adhesion and hemostasis, *Carbohydr. Polym.*, 2019, **208**, 77–85.
20 D. X. Oh, S. Kim, D. Lee and D. S. Hwang, Tunicate-mimetic nanofibrous hydrogel adhesive with improved wet adhesion, *Acta Biomater.*, 2015, **20**, 104–112.
21 H. Ejima, J. J. Richardson, K. Liang, J. P. Best, M. P. Van Koeverden, G. K. Such, J. Cui and F. Caruso, One-Step Assembly of Coordination Complexes for Versatile Film and Particle Engineering, *Science*, 2013, **341**, 154–157.
22 G. Yun, Q. A. Besford, S. T. Johnston, J. J. Richardson, S. Pan, M. Biviano and F. Caruso, Self-Assembly of Nano- to Macroscopic Metal–Phenolic Materials, *Chem. Mater.*, 2018, **30**, 5750–5758.
23 M. A. Rahim, M. Björnmalm, T. Suma, M. Faria, Y. Ju, K. Kempe, M. Müllner, H. Ejima, A. D. Stickland and F. Caruso, Metal–Phenolic Supramolecular Gelation, *Angew. Chem., Int. Ed.*, 2016, **55**, 13803–13807.
24 B. Hu, Y. Shen, J. Adamcik, P. Fischer, M. Schneider, M. J. Loessner and R. Mezzenga, Polyphenol-Binding Amyloid Fibrils Self-Assemble into Reversible Hydrogels with Antibacterial Activity, *ACS Nano*, 2018, **12**, 3385–3396.
25 T. S. Sileika, D. G. Barrett, R. Zhang, K. H. A. Lau and P. B. Messersmith, Colorless Multifunctional Coatings Inspired by Polyphenols Found in Tea, Chocolate, and Wine, *Angew. Chem., Int. Ed.*, 2013, **52**, 10766–10770.
26 K. Liang, J. E. Chung, S. J. Gao, N. Yongvongsoontorn and M. Kurisawa, Highly Augmented Drug Loading and Stability of Micellar Nanocomplexes Composed of Doxorubicin and Poly(ethylene glycol)–Green Tea Catechin Conjugate for Cancer Therapy, *Adv. Mater.*, 2018, **30**, 1706963.
27 N. Yongvongsoontorn, J. E. Chung, S. J. Gao, K. H. Bae, A. Yamashita, M.-H. Tan, J. Y. Ying and M. Kurisawa, Carrier-Enhanced Anticancer Efficacy of Sunitinib-Loaded Green Tea-Based Micellar Nanocomplex beyond Tumor-Targeted Delivery, *ACS Nano*, 2019, **13**, 7591–7602.
28 H. Fan, L. Wang, X. Feng, Y. Bu, D. Wu and Z. Jin, Supramolecular Hydrogel Formation Based on Tannic Acid, *Macromolecules*, 2017, **50**, 666–676.
29 M. Krogsgaard, A. Andersen and H. Birkedal, Gels and threads: mussel-inspired one-pot route to advanced responsive materials, *Chem. Commun.*, 2014, **50**, 13278–13281.
30 L. Zhou, L. Fan, X. Yi, Z. Zhou, C. Liu, R. Fu, C. Dai, Z. Wang, X. Chen, P. Yu, D. Chen, G. Tan, Q. Wang and C. Ning, Soft Conducting Polymer Hydrogels Cross-Linked and Doped by Tannic Acid for Spinal Cord Injury Repair, *ACS Nano*, 2018, **12**, 10957–10967.
31 Y. N. Chen, L. Peng, T. Liu, Y. Wang, S. Shi and H. Wang, Poly(vinyl alcohol)–Tannic Acid Hydrogels with Excellent Mechanical Properties and Shape Memory Behaviors, *ACS Appl. Mater. Interfaces*, 2016, **8**, 27199–27206.
32 M. Shin, J. H. Ryu, J. P. Park, K. Kim, J. W. Yang and H. Lee, DNA/Tannic Acid Hybrid Gel Exhibiting Biodegradability, Extensibility, Tissue Adhesiveness, and Hemostatic Ability, *Adv. Funct. Mater.*, 2015, **25**, 1270–1278.
33 K. Kim, M. Shin, M. Y. Koh, J. H. Ryu, M. S. Lee, S. Hong and H. Lee, TAPE: A Medical Adhesive Inspired by a Ubiquitous Compound in Plants, *Adv. Funct. Mater.*, 2015, **25**, 2402–2410.
34 B. Wang, L. Liu and L. Liao, Light and ferric ion responsive fluorochromic hydrogels with high strength and self-healing ability, *Polym. Chem.*, 2019, **10**, 6481–6488.
35 A. Saha, B. Roy, A. Garai and A. K. Nandi, Two-Component Thermoreversible Hydrogels of Melamine and Gallic Acid, *Langmuir*, 2009, **25**, 8457–8461.
36 Y. Wang, J. P. Park, S. H. Hong and H. Lee, Biologically Inspired Materials Exhibiting Repeatable Regeneration with Self–Sealing Capabilities without External Stimuli or Catalysts, *Adv. Mater.*, 2016, **28**, 9961–9968.
37 M. Shin, E. Park and H. Lee, Plant–Inspired Pyrogallol–Containing Functional Materials, *Adv. Funct. Mater.*, 2019, **29**, 1903022.
38 K. Zhan, C. Kim, K. Sung, H. Ejima and N. Yoshie, Tunicate-Inspired Gallol Polymers for Underwater Adhesive: A Comparative Study of Catechol and Gallol, *Biomacromolecules*, 2017, **18**, 2959–2966.
39 M. Shin and H. Lee, Gallol-Rich Hyaluronic Acid Hydrogels: Shear-Thinning, Protein Accumulation against Concentration Gradients, and Degradation-Resistant Properties, *Chem. Mater.*, 2017, **29**, 8211–8220.
40 J. S. Lee, J. H. Cho, S. An, J. Shin, S. Choi, E. J. Jeon and S. Cho, In Situ Self-Cross-Linkable, Long-Term Stable Hyaluronic Acid Filler by Gallol Autoxidation for Tissue Augmentation and Wrinkle Correction, *Chem. Mater.*, 2019, **31**, 9614–9624.
41 M. Shin, J. H. Galarraga, M. Y. Kwon, H. Lee and J. A. Burdick, Gallol-derived ECM-mimetic adhesive bioinks exhibiting temporal shear-thinning and stabilization behavior, *Acta Biomater.*, 2019, **95**, 165–175.

42 E. M. Euti, A. Wolfel, M. L. Picchio, M. R. Romero, M. Martinelli, R. J. Minari and C. I. A. Igarzabal, Controlled Thermoreversible Formation of Supramolecular Hydrogels Based on Poly(vinyl alcohol) and Natural Phenolic Compounds, *Macromol. Rapid Commun.*, 2019, **40**, 1900217.
43 S. Oliver, O. Vittorio, G. Cirillo and C. Boyer, Enhancing the therapeutic effects of polyphenols with macromolecules, *Polym. Chem.*, 2016, **7**, 1529–1544.
44 C. Locatelli, F. B. Filippin-Monteiro, A. Centa and T. B. Creczinsky-Pasa, Antioxidant, Antitumoral and Anti-Inflammatory Activities of Gallic Acid, in *Handbook on Gallic Acid: Natural Occurrences, Antioxidant Properties and Health Implications*, ed. M. A. Thompson and P. B. Collins, 2013.
45 S. B. Yang, S. H. Yoo, J. S. Lee, J. W. Kim and J. H. Yeum, Surface Properties of a Novel Poly(vinyl alcohol) Film Prepared by Heterogeneous Saponification of Poly(vinyl acetate) Film, *Polymers*, 2017, **9**, 493.
46 S. Kara, C. Tamerler, H. Bermek and Ö. Pekcan, Hysteresis During Sol-Gel and Gel-Sol Phase Transitions of k-Carrageenan: A Photon Transmission Study, *J. Bioact. Compat. Polym.*, 2003, **18**, 33–44.
47 O. N. Tretinnikov and S. A. Zagorskaya, Determination of the degree of crystallinity of poly(vinyl alcohol) by FTIR spectroscopy, *J. Appl. Spectrosc.*, 2012, **79**, 521–526.
48 A. Le Bail, H. Duroy and J. L. Fourquet, Ab-initio structure determination of LiSbWO6 by X-ray powder diffraction, *Mater. Res. Bull.*, 1988, **23**, 447–452.
49 J. Rodríguez-Carvajal, Recent advances in magnetic structure determination by neutron powder diffraction, *Phys. B*, 1993, **192**, 55–69.
50 J. Zhao, I. A. Khan and F. R. Fronczek, Gallic Acid, *Acta Crystallogr., Sect. E: Struct. Rep. Online*, 2011, **67**, 316–317.
51 C. W. Bunn, Crystal Structure of Polyvinyl Alcohol, *Nature*, 1948, **161**, 929–930.
52 S. R. Stauffer and N. A. Peppas, Poly(vinyl alcohol) hydrogels prepared by freezing-thawing cyclic processing, *Polymer*, 1992, **33**, 3932–3936.
53 G. Jiang, C. Liu, X. Liu, Q. Chen, G. Zhang, M. Yang and F. Liu, Network structure and compositional effects on tensile mechanical properties of hydrophobic association hydrogels with high mechanical strength, *Polymer*, 2010, **51**, 1507–1515.
54 H. Yang, S. Xu, L. Jiang and Y. Dan, Thermal Decomposition Behavior of Poly (Vinyl Alcohol) with Different Hydroxyl Content, *J. Macromol. Sci., Part B: Phys.*, 2012, **51**, 464–480.
55 A. Alberti, D. Granato, A. Nogueira, L. I. Mafra, T. A. D. Colman and E. Schnitzler, Modelling the thermal decomposition of 3,4,5-trihydroxybenzoic acid using ordinary least square regression, *Int. Food Res. J.*, 2016, **23**, 30–33.
56 B. Beagley, N. C. Edge, N. Jaiboon, J. J. James, C. A. McAuliffe, M. S. Thorp, M. Watkinson, A. Whiting and D. C. Wright, MM2 force field parameterisation, modelling and structure prediction of salen-type monomeric and hydrogen-bonded dimeric manganese complexes, *Tetrahedron*, 1996, **52**, 10193–10204.
57 Y. Mori, M. Takahashi, Y. Ohno, R. Okura, M. Ishida, T. Higashi, K. Motoyama and H. Arima, Identification of molecular-interaction sites between lowly hydrolyzed polyvinyl alcohols and indomethacin by NMR spectroscopy, *Int. J. Pharm.*, 2018, **549**, 456–465.

